WC Nanocrystals Grown on Vertically Aligned Carbon Nanotubes: An Efficient and Stable Electrocatalyst for Hydrogen Evolution Reaction

Xiujun Fan,*,†,‡,§ Haiqing Zhou,‡,§ and Xia Guo†

†College of Electronic Information and Control Engineering, Beijing University of Technology, Beijing 100124, China and ‡Department of Chemistry, §Richard E. Smalley Institute for Nanoscale Science and Technology, Rice University, Houston, Texas 77005, United States

ABSTRACT Single nanocrystalline tungsten carbide (WC) was first synthesized on the tips of vertically aligned carbon nanotubes (VA-CNTs) with a hot filament chemical vapor deposition (HF-CVD) method through the directly reaction of tungsten metal with carbon source. The VA-CNTs with preservation of vertical structure integrity and alignment play an important role to support the nanocrystalline WC growth. With the high crystallinity, small size, and uniform distribution of WC particles on the carbon support, the formed WC–CNTs material exhibited an excellent catalytic activity for hydrogen evolution reaction (HER), giving a η_{10} (the overpotential for driving a current of 10 mA cm^{-2}) of 145 mV, onset potential of 15 mV, exchange current density@ 300 mV of 117.6 mV and Tafel slope values of 72 mV dec^{-1} in acid solution, and η_{10} of 137 mV, onset potential of 16 mV, exchange current density@ 300 mV of 33.1 mV and Tafel slope values of 106 mV dec^{-1} in alkaline media, respectively. Electrochemical stability test further confirms the long-term operation of the catalyst in both acidic and alkaline media.

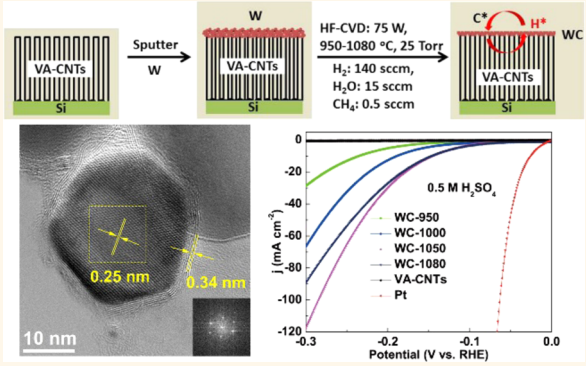

KEYWORDS: nanocrystalline · tungsten carbide · vertically aligned carbon nanotube (VA-CNTs) · hydrogen evolution reaction (HER) · hot filament chemical vapor deposition (HF-CVD)

Hydrogen is considered a promising energy carrier because of its high energy density. Despite its promising future, however, the low-cost, efficient production of hydrogen in a sustainable manner still remains a scientific and technological challenge.[1] One of the most economical ways to produce hydrogen is from water splitting, or hydrogen evolution reaction (HER), which has the ability to store energy without the emission of carbon dioxide.[2] Normally, this process requires a catalyst that minimizes the activation energy of hydrogen formation on the surface. It is well-known that platinum-group metals (PGMs) (Pt, Rh, Pd, *etc.*) are excellent HER electrocatalysts because of their low overpotential and fast kinetics for driving the reaction.[3−5] Unfortunately, the high cost and limited word-wide supply of these noble metals make their application in HER process unattractive. Several non-noble metal materials, such as transition-metal chalcogenides,[6,7] carbides,[8−12] and complexes[13−15] as well as metal alloys[16,17] have been widely investigated recently, and characterized as replacement for PGMs in the evolution of hydrogen. Among them, transition metal carbides, such as molybdenum carbide (Mo_2C)[18−20] and tungsten carbide (WC)[21−26] have been reported to exhibit platinum-like behavior in the catalysis of hydrogenolysis, first by Boudart's group in the 1970s.[27,28] WC exhibits high corrosion resistance and superior electronic conductivity, which makes it a suitable candidate to replace PGM catalysts in emerging renewable energy technologies, such as fuel cells and electrolyzers.[26,29]

The traditional synthesis technique for WC involves heating the fully mixed WO_3 (or W metal) and carbon powder a high temperature (1400−1600 °C).[30] The resultant WC particles are generally big in size, low in specific surface area and poor morphology

* Address correspondence to fxiujun@gmail.com.

Received for review January 20, 2015 and accepted April 13, 2015.

Published online April 13, 2015
10.1021/acsnano.5b00425

control.[31] Numerous methods, such as ball milling,[32] microwave heating,[33] and plasma processing technique,[34] have been developed to obtain nanoscale WC particles. However, these methods remain more or less the following disadvantages: complex procedures, long time, high temperatures and high energy consumption. In particular, Antonietti's group developed a novel synthetic route utilizes organic compounds, such as urea as carbon sources and also utilizes W metal precursors. Unfortunately, the obtain tungsten carbide are still relatively large particles with a low surface area.[31] Most importantly, the purity of WC is not ensured, with WO_x, W_2C or WC_{1-2x} and W metal left with product, which greatly lower the catalytic performance for HER. Up to now, only a few papers were found on the preparation of pure WC.[35,36] Furthermore, hot-filament CVD, one of low temperature CVD techniques,[37] is a common method for growing diamond and diamond-related materials. In the HF-CVD process, the temperature was keep at relatively low temperature, while the filament was heated to over 2000 °C, working as a source of heat for substrate and decomposition of precursor gases.[38] It is cost-effective, easy to scale up to large-scale growth and, no less important, utilizes metal rather than vaporized metal-containing reagents as precursors, which introduce no other impurity. From this point of view, HF-CVD method is the preferable growth technique for pure-phase WC nanostructures.

Carbon nanotubes (CNTs), particularly, vertically aligned carbon nanotubes (VA-CNTs), one of well-studied carbon nanomaterials, have attracted much intention as support for heterogeneous catalyst due to their unique physical properties and morphology. A plethora of literature therefore exists on the functionalization of carbon nanotubes with metal particles.[39] Here, for the first time, we develop a simple and cost-effective method for the preparation of VA-CNTs-supported single nanocrystalline WC (WC−CNTs). A HF-CVD process was employed to generate WC nanoparticles through the directly reaction of metallic tungsten and gaseous activated carbon. In contrast with other methods, the method described here provided a simple technique for one-step synthesis of nanocrystalline WC with hexagonal type structure, uniform dispersion and narrow distribution of sizes. The as-made WC−CNTs material exhibited superior electrocatalytic activity in HER performance, with η_{10} of 145 mV, onset potential of 15 mV and Tafel slop of 72 mV dec^{-1} in acid solution, and 137 mV, 16 mV and 106 mV dec^{-1} in alkaline media, respectively. Furthermore, this preparation technique of metal carbide holds a great potential also for the production of other high melting point metal/carbon supported catalysts.

RESULTS AND DISCUSSION

The experimental setup for the continuous preparation of WC−CNTs is illustrated in Figure 1a. Vertical aligned carbon nanotubes (VA-CNTs) were first grown on silicon substrate according to literature.[40,41] Then, a thin layer of tungsten metal was deposited on top of VA-CNTs with sputter deposition system. After that, HF-CVD process was carried out with 4 tungsten wires hot filament with flowing an activated gas mixture over the sample. Typically, H_2 (140 sccm), H_2O (15 sccm) and CH_4 (0.5 sccm) were rapidly flowed over the hot filament (temperature greater than 2000 °C) at pressures of ~25 Torr to create activated gas of hydrogen and carbon-containing species. During the HF-CVD process, metallic tungsten reacted with gaseous activated carbon species for the nucleation and subsequent growth of WC; meanwhile, VA-CNTs with preservation of vertical structure integrity and alignment were realized. More details are described in Methods. Figures 1b,c show scanning electron microscopy (SEM) images of VA-CNTs carpets before and after growth of WC with HF-CVD method. The original VA-CNTs are highly aligned along the growth directions, and the individual nanotubes are densely packed and uniformly distributed throughout the whole substrate (Figure 1b). Energy-dispersive X-ray spectroscopy (EDS) reveals the presence of only C and litter O (Supporting Information Figure S2a) existed in VA-CNTs, representing high-quality of VA-CNT carpets. After the WC nanocrystals (NCs) growth, the whole assembly of WC−CNTs forest become even denser without collapse or aggregation (Figure 1c). EDS analysis (Supporting Information Figure S2b) indicates that the WC−CNTs consists of C, W and very little O, confirming that tungsten have been carbonized and transformed into tungsten carbide. With increasing of the thickness of tungsten, the grains of WC get more agglomerated. Big NCs of 30−50 nm in diameter are appeared on the top surface of the VA-CNTs when the thickness of tungsten increases to 150 nm (Supporting Information Figure S3). Similar agglomeration phenomena are obtained when the synthesis temperature is increased to 1080 °C (Supporting Information Figure S4c,d).

More insight of the effect of HF-CVD temperature was studied by Raman spectra acquired from the W@VA-CNTs and WC−CNTs samples as presented in Figure 1d. The spectrum of the W@VA-CNTs displays characteristic Raman peaks at 126, 265, 696, 728, 957, and 983 cm^{-1} that can be assigned to WO_3, which likely resulted from surface oxidation of tungsten layer when the sample was exposed to air. A weak band at 1580 cm^{-1} has been attributed to the presence of a small fraction of graphitic carbon in W@VA-CNTs. The weak 2D-band at 2652 cm^{-1} is also detected. With HF-CVD treatment at 950 °C for 6 h, the peaks assigned to WO_3 get weaker. At 1000−1080 °C, the WO_3 peaks are complete vanished, which verify the successful chemical conversion WO_3 and W into WC *via* HF-CVD process. For WC−CNTs samples, the Raman signal may come from VA-CNTs or graphite shell on the WC NCs. The I_G/I_D ratios of WC-composites increase slightly with

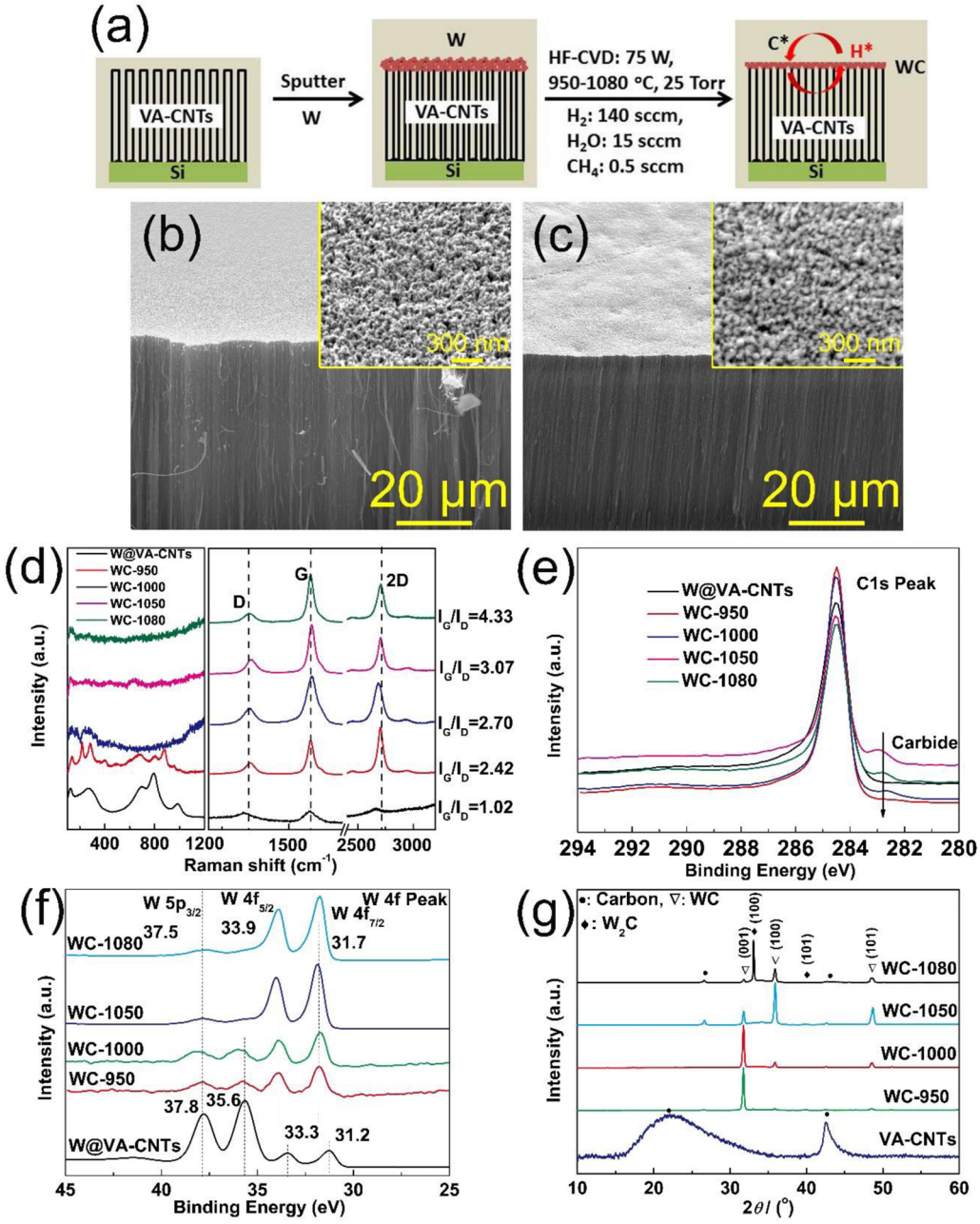

Figure 1. (a) Scheme of the process of WC NCs grown on the tips of VA-CNTs. SEM images of (b) pristine VA-CNTs, (c) resultant WC−CNTs grown at 1050 °C for 6 h. (d) Raman spectrum W@VA-CNTs and WC−CNTs treated with various temperatures for 6 h, the hybrids are denoted by the temperature used in the syntheses (*e.g.*, WC-950, WC-1000, WC-1050 and WC-1080). XPS Spectra of W@VA-CNT and WC−CNTs hybrid obtained at different temperature for (c) C 1s, and (d) W 4f. (g) The XRD patterns of the WC-based products variation of the temperatures with thickness of W 100 nm.

increasing of temperature could be due to atomic hydrogen getting rid of amorphous carbon in VA-CNTs (purification).[42] Another possibility is that the new graphitic shells on the WC NCs obtained at high temperature are low defect.[43] The X-ray photoelectron spectroscopy (XPS) for the synthesized WC−CNTs were also obtained at different temperatures and shown in Figure 1e,f. W@VA-CNTs before HF-CVD process was used as a reference for the comparison of WC grown with various conditions. For W@VA-CNTs and all WC−CNTs samples, main C 1s peaks at 284.7 eV are observed, which originate from VA-CNTs or graphitic shell on the WC NCs (Figure 1e). For WC−CNTs synthesized in the temperature ranged of 1000−1080 °C, the carbide C 1s located at 282.8 eV start to increase, indicating that the increased amount of WC NCs existed in the sample.[29] From Figure 1f, the intensity of W 4f signals assigned to WO_3 species (35.6 and 37.8 eV) decreases with an increase in temperature, whereas the intensity of carbide W 4f signal (31.7 and 33.9 eV) increases with increasing temperature, corresponding again to the concrete formation of WC NCs.

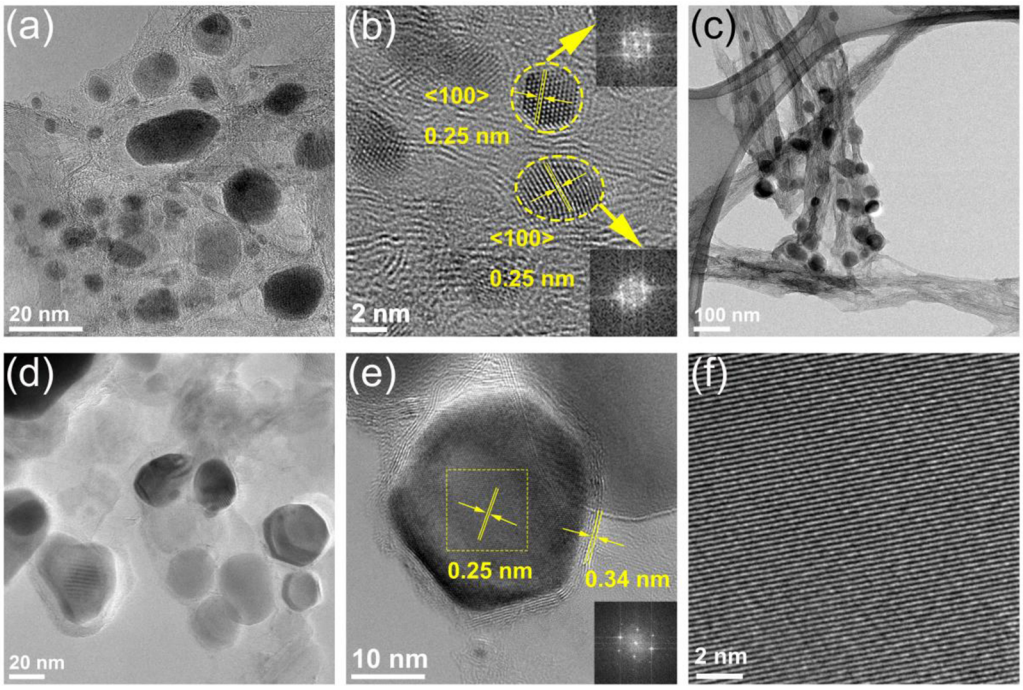

Figure 2. TEM image of WC NCs grown on the tips of VA-CNTs at (a and b) 950 °C for 6 h, (c−f) 1050 °C for 6 h with 100 nm W. (e) TEM images of an individual NCs with the arrows showing lattice fringes of the WC (001) plane, and graphitic shell. The inset of (e) shows a fast Fourier transform (FFT) pattern of the flat surface. (f) TEM image of WC in the enlarge image of the selected area in (e).

The C 1s spectra of WC−CNTs grown at 1050 °C with various thickness of W also show a shoulder at 282.8 eV conforms that WC−CNTs are carbide-terminated even through the thickness of tungsten is up to 150 nm (Supporting Information Figure S5), indicating the efficiency of this HF-CVD method for the growth of WC NCs. Further characterization techniques are employed to characterize WC−CNTs samples grown with different temperatures. Figure 1g reveals XRD patterns of the samples synthesized at 950−1080 °C, while keeping the thickness of deposited W with 100 nm. At relatively low temperature (950 and 1000 °C), only a sharp peak characteristic of hexagonal WC (001) is observed, indicating the formation of small WC particles. At such temperatures, no peaks of W_2C are able to detect in the product. It is noted that there is a clear phase transition at 1050 °C where WC (100) becomes dominate. At higher temperature (1080 °C), the primary diffraction peaks assignable to cubic W_2C are appeared, while both peaks for the WC (100) and (001) are decreased. This W_2C phase has a hexagonal structure with a *P*3*m*1 space group (ICSD-77568), with characteristic diffraction peaks observed at 2 θ = 37.9 (d = 2.368 Å, W_2C (100)). It is considered that W_2C formed as a result of the eutectoid decomposition of WC, in agreement with the W−C phase diagram,[44] where W_2C and WC could coexist above 1050 °C.[45] Supporting Information Figure S6c illustrates XRD patterns of the samples synthesized at a constant temperature of 1050 °C while varying the starting thickness of W. Despite various thickness of tungsten, the product always gives hexagonal WC with a P_{6m2} space group (ICSD-77566), as identified in the XRD pattern, with primary diffraction peaks detected at 2θ = 31.5 (d = 2.858 Å, WC (001)), 35.7 (d = 2.511 Å, WC (100)), and 48.28 (d = 1.887 Å, WC (101)). This result indicates that HF-CVD process is an efficient way to grow WC on the VA-CNTs without pretreatment, and the WC phase could be obtained at temperatures above 950 and below 1080 °C, and W_2C was produced above this temperature.

To further investigate the morphology and crystal structure of formed WC NCs with different HF-CVD temperature (950 and 1080 °C), TEM images were taken and shown in Figure 2. In the literature,[29] the WC phase is commonly referred to as α-WC, and this designation is used here-after. As observed, both WC-950 and WC-1050 are consisted of nanocrystalline WC and CNTs, and the WC NCs lies on the tips of CNTs, with few-layer graphene shell surrounded. The high resolution TEM (HRTEM) and the corresponding FFT images (inset in Figure 2b) reveal that the hexagonal nanocrystalline WC are grown along the zone axis ⟨001⟩. WC-950 NCs are randomly shaped with an average particle size of ∼4.5 nm (Figure 2a,b), whereas WC-1050 samples exhibit a more uniform particle size distribution with an average particle size of ∼21.6 nm (Figure 2c,d). For even higher temperature (1080 °C), the hybrids are obtained with WC NCs size up to 35 nm (Supporting Information Figure S3). The HRTEM images (Figure 2e,f) allow us to observe the crystalline nature of WC NCs produced in more detail. Figure 2e presents

the lattice fringes with a *d*-spacing of 0.25 nm, which is consistent with the one observed in Figure 2b. Enlarged image of selected area in Figure 2e is shown in Figure 2f. No dislocations and distortion can be observed, suggesting that WC NCs are with high quality. The VA-CNTs support preserving of vertical structure integrity plays crucial roles in forming WC NCs, it provides a large surface area for the loaded W-compounds to contact readily with atomic hydrogen and carbon source. These reaction conditions promote the homogeneous nucleation of WC NCs, resulting in a uniform metal carbide distribution over the carbon support.

As to the growth mechanism, we consider that the formation of WC might be based on the reaction of metal tungsten and highly reactive carbon from hot filament activation. In the reaction process, a hot filament (temperature greater than 2000 °C) is employed to create activated gas mixtures consisting of atomic hydrogen (Reaction 1) and carbon-containing species (Reaction 2). WO_x is reduced by atomic hydrogen to produce metal tungsten (Reaction 3);[46] meanwhile, CH_4 is decomposed as active carbon C (noted as C*) (Reaction 2). The newly formed C* is so active that it could directly react with metal tungsten to form WC with high crystallinity at the reaction temperature (Reaction 4). When the temperature is further increased, W_2C starts to form from either direct reaction of W with C* (Reaction 5) or partial decomposition of WC (Reaction 6), which occurs at the high temperatures.[44,47] The possible formation process of WC can be expressed by the following equations:

$$H_2 \rightarrow H^* \quad (1)$$

$$CH_4 \rightarrow C^* + H^* \quad (2)$$

$$WO_x + H^* \rightarrow W + H_2O \quad (3)$$

$$W + C^* \xrightarrow{H^*} WC \quad (4)$$

$$W + C^* \xrightarrow{H^*} W_2C \text{ (higher } T\text{)} \quad (5)$$

$$WC \xrightarrow{H^*} W_2C + C \text{ (higher } T\text{)} \quad (6)$$

According to free energy calculations,[48] the present synthetic route is thermodynamically spontaneous and highly exothermic. Gibbs free energy of W_2C is low at a high temperature.[49] It is reasonable to conclude that W_2C is more likely to be formed than WC at a high temperature; while WC is more stable than W_2C at a low temperature, and WC could be decomposed to W_2C Reaction 6; hence, WC and W_2C exist simultaneously due to thermodynamics of carbide formation free energy.[44] The adding of hot filament step in the synthetic route is critical to the formation of WC NCs. It not only assist to form active carbon that could diffuse into tungsten surface and react with tungsten, but also creates excessive atomic hydrogen environment that activates tungsten surface *via* reduction of WO_x and catalyzes the crystallization of WC.[50]

The electrocatalytic activities of the as-synthesized WC−CNTs toward HER were examined in both acidic (0.5 M H_2SO_4) and alkaline (0.1 M KOH) aqueous solution. The polarization curves (Figure 3a,c) and Tafel plots (Figure 3b,d) without *iR* correction of tungsten carbide synthesized at different temperatures were obtained at a voltage sweeping rate of 50 mV s^{-1}. The overpotential at the cathodic current density of 10 mA cm^{-2}, denoted as η_{10}, can be used to evaluate the HER performance of the catalysts. Electrochemical impedance spectroscopy (EIS) performed at −0.2 V *vs* RHE in Supporting Information Figure S8 exhibit very small series resistances of the as-grown catalysts. The WC-950 gives out the lowest HER catalytic activity, with a Tafel slope 108, 298 mV dec^{-1} and onset potential value of 66, 67 mV in acidic and alkaline medium, respectively. The HER activity is highly enhanced in terms of both Tafel slope and onset potential when the growth temperature increases from 950 to 1050 °C. WC-1050 affords a lower Tafel slope of 72 and 106 mV dec^{-1} in acidic and alkaline medium, respectively, while the onset potential comes to 15 and 16 mV in acidic and alkaline medium, respectively (Supporting Information Table S3). Among the synthesized tungsten-based NCs, WC-1050 has the highest activity with j = 117.6 mA cm^{-2} @300 mV, followed by the WC-1080 sample with an exchange current density of j = 33.1 mA cm^{-2} @300 mV, which is consistent with the polarization curves exhibited in Figure 3a,c. The higher current density observed for the WC-1050 sample could be attributed to the high quality carbide phase which has the Pt-like electronic structure in combination with the high surface area of the material (Supporting Information Table S3). However, as the synthesis temperature increases to 1080 °C, the HER current density decreased. It is worth noting that different carbide phases (W_2C and WC) have different hydrogen reaction mechanism pathways, and WC exhibits better hydrogen evolution performance than W_2C under acidic conditions even though W_2C has a higher surface area.[51] Our results are supported by Armstrong and Bell who found that in acidic electrolyte solutions WC possessed a high HER activity, but W_2C:WC (7:3) mixtures showed an even increased overpotential and a thus worse performance.[52] The decreased of HER performance of WC-1080 most likely result from the introduction of second phase (W_2C), which is consistent with recent DFT and experimental studies on transition-metal carbides.[12] It should be noted that, in alkaline solution, the HER activities of WC based catalysts exhibit excellent electrocatalytic activity as those in acidic solutions and the activity follows the same trend[53] (Figure 3c,d).

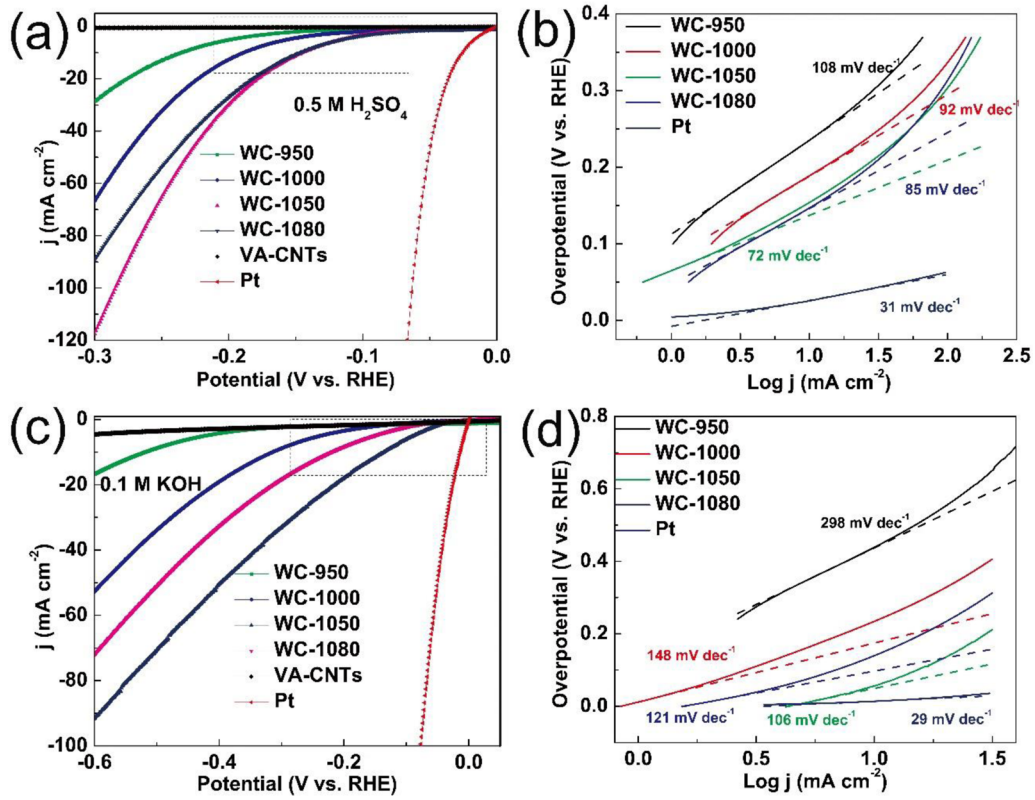

Figure 3. HER voltammograms and the corresponding HER Tafel plots of WC−CNTs synthesized at different temperatures in (a and b) 0.5 M H_2SO_4 (pH = 0) and (c and d) 0.1 M KOH (pH = 13). The enlargement of the rectangle regions near the onset potential in panels a and c are shown in Supporting Information.

It suggests that WC- based catalyst is favorable to facilitate water dissociate step in alkaline solution. WC−CNTs has the same HER mechanism under both two conditions.

The variation of onset potentials determined from the inflection points of the polarization curves, with η at 10 mA cm^{-2}, current density @300 mV, and the Tafel slopes over W thickness with sputter are shown in Figure 4a,b. The η_{10}, onset potential, and Tafel slope for WC 100 nm are 145 mv, 15 mV, and 72 mV dec^{-1} in acidic medium, and 137 mv, 16 mV, and 106 mV dec^{-1} in alkaline solution respectively, which are significantly lower than that of W 50 nm (207 mV, 76 mV and 102 mV dec^{-1} in acidic medium, and 289 mV, 64 mV and 185 mV dec^{-1} in alkaline solution), indicating the greatly enhanced HER activity with increasing the depositing W thickness. Increasing the depositing W thickness means more WC loading. The HER performance enhanced along with the increase of W thickness because of the raise in the number active sites available for hydrogen evolution introduced by more WC loading. The even higher exchange current @ 300 mV for WC 100 nm indicates better HER activity, in good agreement with the higher concentration of exposed edges and small dimension in the W 100 nm. When the thickness of tungsten was increased to 150 nm, the HER activity is degraded, showing a *j*@ 300 mV of ~71 mA and onset potential of 22 mV in acidic solution. Too much tungsten form large WC NCs, and the lager NCs guarantee worse electrical conductivity from the substrate to the surface sites,[54] which in turn limit the charge transfer process and lower the HER activity. Moreover, with given temperature and growth time, the thicker of the tungsten layer leads larger WC NCs, which afford less accessible reactive sites.[11] So decreasing HER activity could also be due to a decrease in the active edge with lager particles. The fluent charge transport could also be characterized by electrochemical impedance spectroscopy (EIS), as illustrated in Supporting Information Figure S8. WC−CNTs hybrid catalyst exhibits very low charge transfer resistance (R_{CT}) (Supporting Information Table S3). Furthermore, the small series resistances observed for all samples (~8 Ω) shows the importance of the direct synthesis on conductive substrates, which enables simple and effective electrical integration that minimized parasitic Ohmic losses. The superior performances of WC based catalyst are attributed high quality, sufficient active sites as well as the relatively low resistance of the electrode.

Catalytic stability is another significant criterion for HER catalysts. To evaluate the durability of the WC−CNTs catalyst, continuous HER at static overpotential and a long-term cycling tests were conducted in an acidic and alkaline environment, respectively. In acidic solution (0.5 M H_2SO_4), the catalyst current density

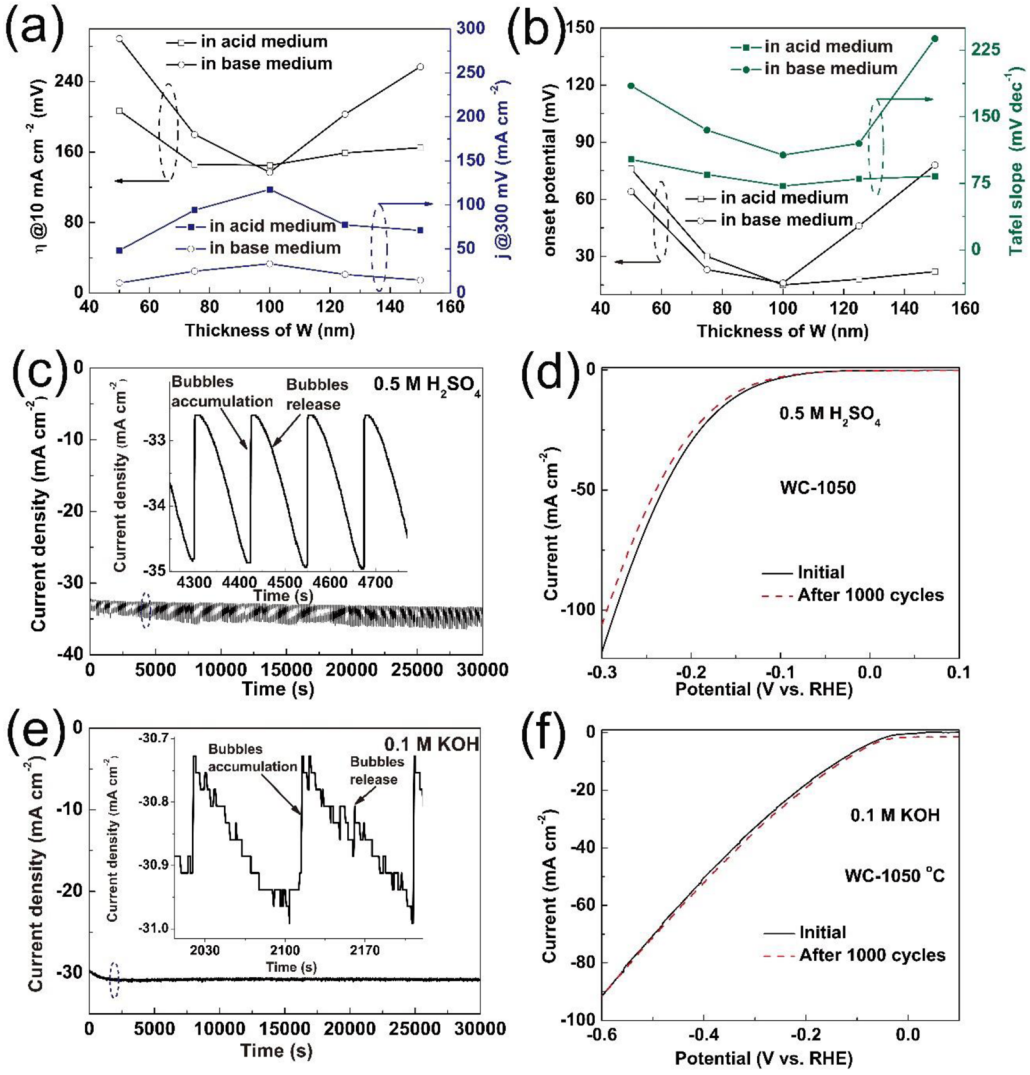

Figure 4. (a) The variation of overpotential at 10 mA cm^{-2} and current density @300 mV on W thickness with sputter, respectively. (b) The variation of onset potential and Tafel slope on W thickness with sputter, respectively. (c and e) Time dependence of current density during electrolysis over 30 000 s at fixed overpotentials of −155, −173 mV in acidic and alkaline medium, respectively. Insets: enlargement of the area denoted by the dash circles. (d and f) The first and 1000th polarization cycles for the WC-1050 sample in acidic and alkaline medium, respectively.

remains stable at ~20 mA cm^{-2} for electrolysis over 30 000 s (Figure 4c). As seen in Figure 4e, in alkaline medium (0.1 M KOH), at higher overpotentials to drive high current densities of ~50 mA cm^{-2}, a little increase in cathodic current density of about 10% is observed in the WC−CNTs electrodes during the first 1 h. The catalytic current then fully stabilizes for the rest of the potentiostatic electrolysis. The as-measured time-dependent curve is in typical serrate shape, which can be attributed to the alternate processes of bubble accumulation and bubble release (insets of Figure 4c,e). This exceptional durability demonstrates promise for practical applications of the catalysts over the long-term. WC−CNTs exhibits excellent electrochemical stability with negligible degradations after 30 000 s testing, suggesting that the WC NCs bind strongly on the CNTs substrate through the HF-CVD process.[54] A long-term cycling test was also performed to assess the electrochemical stability. The catalytic stability of WC−CNTs catalyst was characterized by continuous cyclic voltammetry performed between −0.2 and 0.2 V *vs* RHE at 50 m s^{-1} scan rate (Figure 4d,f). Only a minor deterioration of cathodic current is observed after 1000 cycling in both 0.5 M H_2SO_4 and 0.1 M KOH solutions. This finding clearly indicates the high stability of the carbide material with strong tolerance to both acidic and alkaline solution. Earlier work has disclosed that when exposed to aqueous solutions, WC undergoes continuous oxidation, thus showing not good stability.[55,56] In our case, such a high activity and stability of the WC−CNTs hybrid should originate from (i) the synergistic effect between WC and CNTs, as the graphitic shell covered WC can enhance the electrical conductivity, improve the stability of the hybrid as a protective layer, and provide more active sites.[57] (ii) The VA-CNTs provide high surface area to contact with

electrolyte, and dispersed the W-compound nanoparticles without aggregation. With the high crystallinity, small size and uniform distribution of WC NCs on the carbon support, the WC−CNTs composite could substantially increase the number of active sites (contact area between metal carbides and electrolyte) and the unit activity of each site (by enhanced electron transfer), and thus offer the enhanced activity of for HER.

CONCLUSIONS

High quality and pure phase WC NCs with a size of approximately 4.5−21.6 nm on the tips of VA-CNTs were successfully synthesized. The final size of the NCs could be controlled through a simple modification by varying the amount of W and growth conditions. Electrochemical studies showed that the WC-1050 sample exhibited the highest and most stable HER activity in both acidic and alkaline medium among the samples prepared in this study. The obtained η_{10}, onset potential, and Tafel slope values of WC-1050 were 145 mV, 15 mV, and 72 mV dec^{-1} in acid solution, and 137 mV, 16 mV, and 106 mV dec^{-1} in alkaline media, respectively. The WC−CNTs catalyst featured a robust stability in both acidic and alkaline aqueous solution without corrosion and oxidation. Although the performance of our samples is not yet comparable to that of platinum, this study introduces the great potential of tungsten carbide grown with HF-CVD method as a non-noble-metal alternative for use as a cathode catalyst in hydrogen evolution reduction.

METHODS

Synthesis of VA-CNTs Carpets. The VA-CNTs carpets were synthesized was synthesized as previously reported. Briefly, the substrate for growing VA-CNTs carpets was prepared by electron-beam evaporating a 10 nm Al_2O_3 buffer layer and 0.8 nm Fe catalyst layer sequentially onto the silicon wafer in an electron-beam evaporator. Typically, a mixture of H_2 (210 sccm), C_2H_2 (2 sccm) and H_2O (200 sccm) gas was flowed into the reactor at 750 °C with an elevated pressure (~25 Torr). Usually, a tungsten hot filament was activated with a power of 30 W for 30 s to reduce the catalysts by generating atomic hydrogen in order to initiate the VA-CNT nucleation. The pressure was then decreased immediately to 6.4 Torr to resume the VA-CNTs carpets growth. A 15 min-growth process enabled a vertical VA-CNTs carpet with a height of 120−150 μm.

WC Nanoparticle Synthesis. In a typical synthesis, a layer of tungsten (50−150 nm) was deposited on the tips of carbon nanotubes vertically array with sputter system. The VA-CNTs carpets with a layer of tungsten were loaded into the CVD furnace chamber below the hot filament about 3−6 mm. The hot filament was located near the center of the furnace and the center of a 25 mm diameter quartz tube. The filament was ~8 mm long and made from 10 mill tungsten wire. And 4 tungsten wires were used to make a filament array assembly. Filaments were brought up to the operating temperature over ~10 min to allow for filament carburization. Typically, atomic hydrogen treatment was carried out using a mixture of H_2 (140 sccm), H_2O (15 sccm) and CH_4 (0.5 sccm) at 25 Torr for 1−9 h. The temperature was varied from 950 to 1080 °C. And the hot filament power was keep at 75 W. Finally, the sample was naturally cooling to room temperature by turning off the power supply to the hot filament and furnace. After growth, the WC−CNTs, were detached from the Si wafer simply by peeling off from the Si substrate using a razor blade.

Characterization of the Templates and Catalysts. A Bruker D_8 Advance diffractometer (DMAX 2500) operating with a Cu Kα energy source at 40 kV and 40 mA was used to crystallographically characterize the materials. The XPS spectra were calibrated against the C 1s photoelectron signal at 285 eV on an Amicus/ESCA 3400 from Kratos Analytical instrument operating with dual Mg/Al anodes with an energy source at 12 kV and 10 mA. TGA was performed in a Mettler-Toledo TGA/DSC1 Star system under air (100 mL min^{-1}). BET surface area was measured on a Quantachrome autosorb-3b BET surface analyzer. The samples were prepared by suspending them in ethanol and dispersing them by sonication. A drop of the solution was poured onto a copper-grid-supported carbon film. Then, the grid was dried in air prior to observation. A field-emission TEM (JEOL 2010F) with an imaging filter (Gatan GIF) was used at 200 kV to characterize the morphology and the particle size distribution of the synthesized products. Bath sonication, tip sonication and low-speed centrifugation were used to separate WC from CNTs. The ethanol suspensions of WC were transferred to the surfaces of freshly exfoliated mica, and analyzed using the atom force microscopy (AFM, Digital Instrument Nanoscope IIIA).

Electrochemical Measurements. The HER activity of various WC−CNTs hybrids were performed in argon-purged 0.5 M H_2SO_4 and 0.1 M KOH at room temperature using a standard three-electrode setup employing a mercury/mercurous sulfate reference electrode (CHI 151, CH Instruments Inc., Austin, TX) was used as the reference electrode. A Pt foil (100% Pt, 5 × 10 mm, SPI Supplies, West Chester, PA) was used as the counter electrode. The acquired currents were tentatively normalized by the surface area calculated from the Levich analysis. Hg/HgO (0.1 M KOH) (MMO, 0.098 V *vs* SHE) was used as the reference electrode. All potentials were referenced to a reversible hydrogen electrode (RHE) by adding a value of (0.098 + 0.059 × pH) V. Prior to all measurements, the electrochemical cell was bubbled for 30 min with H_2. To condition the electrodes, 25 CV cycles were conducted between 0.0 V (*vs* the normal hydrogen electrode, NHE) and the onset of oxidation at 50 mV s^{-1}. Tafel curves were then obtained from linear sweep voltammograms using a scan rate of 50 mV s^{-1}. Homogeneity of the platinum-modified surfaces was confirmed by the observation of uniform H_2 gas evolution from the electrode surfaces.

Conflict of Interest: The authors declare no competing financial interest.

Acknowledgment. The authors acknowledge Prof. James M. Tour and Dr. Robert H. Hauge at Rice University for providing research facilities, helpful discussions and assistance, Xiaowei He for assisting in electron-beam evaporation, Zhiwei Peng, Yang Yang, Ruquan Ye, Lei Li, and Jian Lin for helpful discussions, and the China Scholarship Council for partial support of this research.

Supporting Information Available: Materials, WC nanocrystals synthesis and characterizations, and their electrochemical measurements; Table S1−S3; Figures S1−S11. This material is available free of charge *via* the Internet at http://pubs.acs.org.

REFERENCES AND NOTES

1. Greeley, J.; Jaramillo, T. F.; Bonde, J.; Chorkendorff, I.; Norskov, J. K. Computational High-Throughput Screening of Electrocatalytic Materials for Hydrogen Evolution. *Nat. Mater.* **2006**, *5*, 909–913.
2. Khaselev, O.; Turner, J. A. A Monolithic Photovoltaic-Photoelectrochemical Device for Hydrogen Production *via* Water Splitting. *Science* **1998**, *280*, 425–427.

3. Pavel, C. C.; Cecconi, F.; Emiliani, C.; Santiccioli, S.; Scaffidi, A.; Catanorchi, S.; Comotti, M. Highly Efficient Platinum Group Metal Free Based Membrane-Electrode Assembly for Anion Exchange Membrane Water Electrolysis. *Angew. Chem.* **2014**, *126*, 1402–1405.
4. Hou, Y.; Laursen, A. B.; Zhang, J.; Zhang, G.; Zhu, Y.; Wang, X.; Dahl, S.; Chorkendorff, I. Layered Nanojunctions for Hydrogen-Evolution Catalysis. *Angew. Chem., Int. Ed.* **2013**, *52*, 3621–3625.
5. Cheng, L.; Huang, W.; Gong, Q.; Liu, C.; Liu, Z.; Li, Y.; Dai, H. Ultrathin WS_2 Nanoflakes as a High-Performance Electrocatalyst for the Hydrogen Evolution Reaction. *Angew. Chem., Int. Ed.* **2014**, *53*, 7860–7863.
6. Chen, W. F.; Sasaki, K.; Ma, C.; Frenkel, A. I.; Marinkovic, N.; Muckerman, J. T.; Zhu, Y.; Adzic, R. R. Hydrogen-Evolution Catalysts Based on Non-Noble Metal Nickel-Molybdenum Nitride Nanosheets. *Angew. Chem., Int. Ed.* **2012**, *51*, 6131–6135.
7. Voiry, D.; Salehi, M.; Silva, R.; Fujita, T.; Chen, M.; Asefa, T.; Shenoy, V. B.; Eda, G.; Chhowalla, M. Conducting MoS_2 Nanosheets as Catalysts for Hydrogen Evolution Reaction. *Nano Lett.* **2013**, *13*, 6222–6227.
8. Hsu, I. J.; Kimmel, Y. C.; Jiang, X.; Willis, B. G.; Chen, J. G. Atomic Layer Deposition Synthesis of Platinum-Tungsten Carbide Core-Shell Catalysts for the Hydrogen Evolution Reaction. *Chem. Commun.* **2012**, *48*, 1063–1065.
9. Vrubel, H.; Hu, X. Molybdenum Boride and Carbide Catalyze Hydrogen Evolution in Both Acidic and Basic Solutions. *Angew. Chem.* **2012**, *124*, 12875–12878.
10. Wan, C.; Regmi, Y. N.; Leonard, B. M. Multiple Phases of Molybdenum Carbide as Electrocatalysts for the Hydrogen Evolution Reaction. *Angew. Chem.* **2014**, *126*, 6525–6528.
11. Yan, Y.; Xia, B.; Qi, X.; Wang, H.; Xu, R.; Wang, J.-Y.; Zhang, H.; Wang, X. Nano-Tungsten Carbide Decorated Graphene as Co-Catalysts for Enhanced Hydrogen Evolution on Molybdenum Disulfide. *Chem. Commun.* **2013**, *49*, 4884–4886.
12. Esposito, D. V.; Hunt, S. T.; Kimmel, Y. C.; Chen, J. G. A New Class of Electrocatalysts for Hydrogen Production from Water Electrolysis: Metal Monolayers Supported on Low-Cost Transition Metal Carbides. *J. Am. Chem. Soc.* **2012**, *134*, 3025–3033.
13. Xu, Y.; Wu, R.; Zhang, J.; Shi, Y.; Zhang, B. Anion-Exchange Synthesis of Nanoporous FeP Nanosheets as Electrocatalysts for Hydrogen Evolution Reaction. *Chem. Commun.* **2013**, *49*, 6656–6658.
14. Jeong, S.; Yoo, D.; Jang, J.-t.; Kim, M.; Cheon, J. Well-Defined Colloidal 2-D Layered Transition-Metal Chalcogenide Nanocrystals *via* Generalized Synthetic Protocols. *J. Am. Chem. Soc.* **2012**, *134*, 18233–18236.
15. Zhang, J.; Zhu, Z.; Tang, Y.; Müllen, K.; Feng, X. Titania Nanosheet-Mediated Construction of a Two-Dimensional Titania/Cadmium Sulfide Heterostructure for High Hydrogen Evolution Activity. *Adv. Mater.* **2014**, *26*, 734–738.
16. Cao, B.; Veith, G. M.; Neuefeind, J. C.; Adzic, R. R.; Khalifah, P. G. Mixed Close-Packed Cobalt Molybdenum Nitrides as Non-Noble Metal Electrocatalysts for the Hydrogen Evolution Reaction. *J. Am. Chem. Soc.* **2013**, *135*, 19186–19192.
17. Kong, D.; Wang, H.; Lu, Z.; Cui, Y. $CoSe_2$ Nanoparticles Grown on Carbon Fiber Paper: An Efficient and Stable Electrocatalyst for Hydrogen Evolution Reaction. *J. Am. Chem. Soc.* **2014**, *136*, 4897–4900.
18. Weidman, M. C.; Esposito, D. V.; Hsu, Y.-C.; Chen, J. G. Comparison of Electrochemical Stability of Transition Metal Carbides (WC, W_2C, Mo_2C) Over a Wide pH Range. *J. Power Sources* **2012**, *202*, 11–17.
19. Ge, C.; Jiang, P.; Cui, W.; Pu, Z.; Xing, Z.; Asiri, A. M.; Obaid, A. Y.; Sun, X.; Tian, J. Shape-Controllable Synthesis of Mo_2C Nanostructures as Hydrogen Evolution Reaction Electrocatalysts with High Activity. *Electrochim. Acta* **2014**, *134*, 182–186.
20. Liao, L.; Wang, S.; Xiao, J.; Bian, X.; Zhang, Y.; Scanlon, M. D.; Hu, X.; Tang, Y.; Liu, B.; Girault, H. H. A Nanoporous Molybdenum Carbide Nanowire as an Electrocatalyst for Hydrogen Evolution Reaction. *Energy Environ. Sci.* **2014**, *7*, 387–392.
21. Kelly, T. G.; Hunt, S. T.; Esposito, D. V.; Chen, J. G. Monolayer Palladium Supported on Molybdenum and Tungsten Carbide Substrates as Low-Cost Hydrogen Evolution Reaction (HER) Electrocatalysts. *Int. J. Hydrogen Energy* **2013**, *38*, 5638–5644.
22. Kimmel, Y. C.; Esposito, D. V.; Birkmire, R. W.; Chen, J. G. Effect of Surface Carbon on the Hydrogen Evolution Reactivity of Tungsten Carbide (WC) and Pt-modified WC Electrocatalysts. *Int. J. Hydrogen Energy* **2012**, *37*, 3019–3024.
23. Berglund, S. P.; He, H.; Chemelewski, W. D.; Celio, H.; Dolocan, A.; Mullins, C. B. p-Si/W_2C and p-Si/W_2C/Pt Photocathodes for the Hydrogen Evolution Reaction. *J. Am. Chem. Soc.* **2014**, *136*, 1535–1544.
24. Esposito, D. V.; Hunt, S. T.; Stottlemyer, A. L.; Dobson, K. D.; McCandless, B. E.; Birkmire, R. W.; Chen, J. G. Low-Cost Hydrogen-Evolution Catalysts Based on Monolayer Platinum on Tungsten Monocarbide Substrates. *Angew. Chem., Int. Ed.* **2010**, *49*, 9859–9862.
25. Hunt, S. T.; Nimmanwudipong, T.; Román-Leshkov, Y. Engineering Non-sintered, Metal-Terminated Tungsten Carbide Nanoparticles for Catalysis. *Angew. Chem., Int. Ed.* **2014**, *53*, 5131–5136.
26. Yan, Y.; Zhang, L.; Qi, X.; Song, H.; Wang, J. Y.; Zhang, H.; Wang, X. Template-Free Pseudomorphic Synthesis of Tungsten Carbide Nanorods. *Small* **2012**, *8*, 3350–3356.
27. Levy, R.; Boudart, M. Platinum-Like Behavior of Tungsten Carbide in Surface Catalysis. *Science* **1973**, *181*, 547–549.
28. Ribeiro, F.; Dalla Betta, R.; Guskey, G.; Boudart, M. Preparation and Surface Composition of Tungsten Carbide Powders with High Specific Surface Area. *Chem. Mater.* **1991**, *3*, 805–812.
29. Hunt, S. T.; Nimmanwudipong, T.; Román-Leshkov, Y. Engineering Non-Sintered, Metal-Terminated Tungsten Carbide Nanoparticles for Catalysis. *Angew. Chem., Int. Ed.* **2014**, *53*, 5131–5136.
30. Wu, Z.; Yang, Y.; Gu, D.; Li, Q.; Feng, D.; Chen, Z.; Tu, B.; Webley, P. A.; Zhao, D. Silica-Templated Synthesis of Ordered Mesoporous Tungsten Carbide/Graphitic Carbon Composites with Nanocrystalline Walls and High Surface Areas *via* a Temperature-Programmed Carburization Route. *Small* **2009**, *5*, 2738–2749.
31. Giordano, C.; Erpen, C.; Yao, W.; Antonietti, M. Synthesis of Mo and W Carbide and Nitride Nanoparticles *via* a Simple "Urea Glass" Route. *Nano Lett.* **2008**, *8*, 4659–4663.
32. Wang, G.; Campbell, S.; Calka, A.; Kaczmarek, W. Synthesis and Structural Evolution of Tungsten Carbide Prepared by Ball Milling. *J. Mater. Sci.* **1997**, *32*, 1461–1467.
33. Lu, J. L.; Li, Z. H.; Jiang, S. P.; Shen, P. K.; Li, L. Nanostructured Tungsten Carbide/Carbon Composites Synthesized by a Microwave Heating Method as Supports of Platinum Catalysts for Methanol Oxidation. *J. Power Sources* **2012**, *202*, 56–62.
34. Cha, S. I.; Hong, S. H.; Ha, G. H.; Kim, B. K. Mechanical Properties of WC-10Co Cemented Carbides Sintered from Nanocrystalline Spray Conversion Processed Powders. *Int. J. Refract. Met. Hard Mater.* **2001**, *19*, 397–403.
35. Engqvist, H.; Ederyd, S.; Axen, N.; Hogmark, S. Grooving Wear of Single-Crystal Tungsten Carbide. *Wear* **1999**, *230*, 165–174.
36. Nie, M.; Shen, P. K.; Wei, Z.; Li, Q.; Bi, H.; Liang, C. Preparation of Pure Tungsten Carbide and Catalytic Activity of Platinum on a Tungsten Carbide Nanocrystalline Support for Oxygen Reduction. *ECS Electrochem. Lett.* **2012**, *1*, H11–H13.
37. Chong, S. K.; Goh, B. T.; Dee, C. F.; Rahman, S. A. Study on the Role of Filament Temperature on Growth of Indium-Catalyzed Silicon Nanowires by the Hot-Wire Chemical Vapor Deposition Technique. *Mater. Chem. Phys.* **2012**, *135*, 635–643.
38. Ali, M.; Urgen, M.; Atta, M. A. Tantalum Carbide Films Synthesized by Hot-filament Chemical Vapor Deposition Technique. *Surf. Coat. Technol.* **2012**, *206*, 2833–2838.
39. Planeix, J.; Coustel, N.; Coq, B.; Brotons, V.; Kumbhar, P.; Dutartre, R.; Geneste, P.; Bernier, P.; Ajayan, P. Application of Carbon Nanotubes as Supports in Heterogeneous Catalysis. *J. Am. Chem. Soc.* **1994**, *116*, 7935–7936.

40. Xu, Y.-Q.; Flor, E.; Kim, M. J.; Hamadani, B.; Schmidt, H.; Smalley, R. E.; Hauge, R. H. Vertical Array Growth of Small Diameter Single-Walled Carbon Nanotubes. *J. Am. Chem. Soc.* **2006**, *128*, 6560–6561.
41. Pint, C. L.; Sun, Z.; Moghazy, S.; Xu, Y.-Q.; Tour, J. M.; Hauge, R. H. Supergrowth of Nitrogen-Doped Single-Walled Carbon Nanotube Arrays: Active Species, Dopant Characterization, and Doped/Undoped Heterojunctions. *ACS Nano* **2011**, *5*, 6925–6934.
42. Talyzin, A. V.; Luzan, S.; Anoshkin, I. V.; Nasibulin, A. G.; Jiang, H.; Kauppinen, E. I.; Mikoushkin, V. M.; Shnitov, V. V.; Marchenko, D. E.; Noréus, D. Hydrogenation, Purification, and Unzipping of Carbon Nanotubes by Reaction with Molecular Hydrogen: Road to Graphane Nanoribbons. *ACS Nano* **2011**, *5*, 5132–5140.
43. Zhang, H.; Liang, C.; Liu, J.; Tian, Z.; Shao, G. The Formation of Onion-Like Carbon-Encapsulated Cobalt Carbide Core/Shell Nanoparticles by the Laser Ablation of Metallic Cobalt in Acetone. *Carbon* **2013**, *55*, 108–115.
44. Kurlov, A.; Gusev, A. Tungsten Carbides and WC Phase Diagram. *Inorg. Mater.* **2006**, *42*, 121–127.
45. Fang, Z. Z.; Wang, X.; Ryu, T.; Hwang, K. S.; Sohn, H. Y. Synthesis, Sintering, and Mechanical Properties of Nanocrystalline Cemented Tungsten Carbide – A Review. *Int. J. Refract. Met. Hard Mater.* **2009**, *27*, 288–299.
46. Löfberg, A.; Frennet, A.; Leclercq, G.; Leclercq, L.; Giraudon, J. Mechanism of WO_3 Reduction and Carburization in CH_4/H_2 Mixtures Leading to Bulk Tungsten Carbide Powder Catalysts. *J. Catal.* **2000**, *189*, 170–183.
47. Savarimuthu, A. C.; Taber, H. F.; Megat, I.; Shadley, J. R.; Rybicki, E. F.; Cornell, W. C.; Emery, W. A.; Somerville, D. A.; Nuse, J. D. Sliding Wear Behavior of Tungsten Carbide Thermal Spray Coatings for Replacement of Chromium Electroplate in Aircraft Applications. *J. Therm. Spray Technol.* **2001**, *10*, 502–510.
48. Gupta, D. K.; Seigle, L. L. Free Energies of Formation of WC and W_2C, and the Thermodynamic Properties of Carbon in Solid Tungsten. *Metall. Trans. A* **1975**, *6*, 1939–1944.
49. Li, J.; Li, H.; Wang, M.; Wang, S.; Ji, Q.; Li, M.; Chi, J. Applications of WC-based Composites Rapid Synthesized by Consumable Electrode *in-situ* Metallurgy to Cutting Pick. *Int. J. Refract. Met. Hard Mater.* **2012**, *35*, 132–137.
50. Decker, S.; Löfberg, A.; Bastin, J.-M.; Frennet, A. Study of the Preparation of Bulk Tungsten Carbide Catalysts with C_2H_6/H_2 and C_2H_4/H_2 Carburizing Mixtures. *Catal. Lett.* **1997**, *44*, 229–239.
51. Garcia-Esparza, A. T.; Cha, D.; Ou, Y.; Kubota, J.; Domen, K.; Takanabe, K. Tungsten Carbide Nanoparticles as Efficient Cocatalysts for Photocatalytic Overall Water Splitting. *ChemSusChem* **2013**, *6*, 168–181.
52. Armstrong, R.; Bell, M. Tungsten Carbide Catalysts for Hydrogen Evolution. *Electrochim. Acta* **1978**, *23*, 1111–1115.
53. Zheng, Y.; Jiao, Y.; Li, L. H.; Xing, T.; Chen, Y.; Jaroniec, M.; Qiao, S. Z. Toward Design of Synergistically Active Carbon-Based Catalysts for Electrocatalytic Hydrogen Evolution. *ACS Nano* **2014**, *8*, 5290–5296.
54. Wang, H.; Lu, Z.; Kong, D.; Sun, J.; Hymel, T. M.; Cui, Y. Electrochemical Tuning of MoS_2 Nanoparticles on Three-Dimensional Substrate for Efficient Hydrogen Evolution. *ACS Nano* **2014**, *8*, 4940–4947.
55. Voorhies, J. D. Electrochemical and Chemical Corrosion of Tungsten Carbide (WC). *J. Electrochem. Soc.* **1972**, *119*, 219–222.
56. Yang, Y.; Fei, H.; Ruan, G.; Xiang, C.; Tour, J. M. Edge-Oriented MoS_2 Nanoporous Films as Flexible Electrodes for Hydrogen Evolution Reactions and Supercapacitor Devices. *Adv. Mater.* **2014**, *26*, 8163–8168.
57. Hou, Y.; Huang, T.; Wen, Z.; Mao, S.; Cui, S.; Chen, J. Metal-Organic Framework-Derived Nitrogen-Doped Core-Shell-Structured Porous Fe/Fe_3C@C Nanoboxes Supported on Graphene Sheets for Efficient Oxygen Reduction Reactions. *Adv. Energy Mater.* **2014**, *4*, 1400337.